Influence of Lap Splices on the Deformation Capacity of RC Walls. II: Shell Element Simulation and Equivalent Uniaxial Model

Danilo Tarquini[1]; João P. Almeida[2]; and Katrin Beyer, M.ASCE[3]

Abstract: Spliced longitudinal reinforcement may result in a reduction of both strength and displacement capacity of reinforced concrete (RC) members. This applies in particular when lap splices are located in regions where inelastic deformations concentrate, such as the plastic zone at the base of RC walls. This paper introduces a simple numerical model suitable for engineering practice to simulate the force-displacement response of RC walls with lap splices. Based on experimental data from 16 test units, an equivalent uniaxial steel stress-strain law is proposed that represents the monotonic envelope of the cyclic response of spliced rebars in RC walls up to the onset of strength degradation. It allows for modeling lap splice response with finite element (FE) models while avoiding the use of complex interface bond-slip elements. A new semi-empirical expression for the strain at the onset of strength degradation is derived, which expresses the strain capacity of the lap splice as a function of the confining reinforcement ratio and the ratio of lap splice length to shear span of the wall. The proposed equivalent constitutive law was included in shell element models to predict the force-displacement response of the test unit set of RC walls. Results demonstrated the ability of this approach to adequately capture the peak strength and displacement capacity of the spliced units. **DOI: 10.1061/(ASCE)ST.1943-541X.0001859.**

Author keywords: Seismic effects; Reinforced concrete walls; Lap splice; Equivalent uniaxial model.

Introduction

Most performance-based assessment approaches are based on the comparison between the structural displacement capacity and the expected demand. In new reinforced concrete (RC) structures, the capacity design philosophy (Paulay and Priestley 1992; Priestley et al. 2007) ensures that the response is governed by a ductile flexural mechanism. Estimating the displacement capacity of existing structures is a more challenging task because a large number of failure modes and deformation components need to be considered (Syntzirma and Pantazopoulou 2006). In particular, the displacement capacity of a structural member can be substantially reduced by detailing deficiencies such as insufficient shear reinforcement, insufficient confinement of boundary elements, or the presence of spliced longitudinal reinforcement.

This paper addresses the detrimental effect of lap splices in the cyclic behavior of RC walls, which may adversely affect the overall structural seismic response. While the force capacity of lap splices has been extensively studied in the past, their deformation ductility was only addressed in a limited number of investigations. Lap splice strain limits were developed in the framework of plastic hinge analysis, which will be reviewed in this paper. The present work aims at complementing previous studies by proposing a new equivalent steel stress-strain relationship for the behavior of spliced rebars in RC walls. The latter can be used in numerical simulations avoiding the need for complex interface bond-slip models in finite element (FE) analysis (typically required to account for the slip of the reinforcement with respect to the surrounding concrete), thus resulting in a suitable tool for engineering practice. The derived monotonic constitutive model, which intends to be an envelope of the cyclic response of lap splices up to the onset of strength degradation, is built from two defining points representing an equivalent yield and an ultimate condition. The yield point is related to the lap splice strength, for which the existing large number of literature proposals are first reviewed and subsequently applied to the spliced RC walls of the database collected in Table 1 of the companion paper (Almeida et al. 2017), which includes 16 walls with lap splices plus eight reference units with continuous reinforcement. The ultimate strain capacity describes instead the point of strength degradation onset triggered by the presence of lap splices in the structural member and is obtained from regression analysis of the response of the 16 spliced units. Finally, the validation of the proposed equivalent constitutive law is carried out by combining it with shell element models to simulate the force-displacement response of the complete set of RC walls.

State-of-the-Art Models for Lap Splice Behavior

The majority of previous studies on lap splice response concentrated on lap splice strength rather than lap splice deformation

[1]Ph.D. Candidate, Earthquake Engineering and Structural Dynamics Laboratory, School of Architecture, Civil and Environmental Engineering, École Polytechnique Fédérale de Lausanne, EPFL ENAC IIC EESD, GC B2 495, Station 18, CH-1015 Lausanne, Switzerland (corresponding author). E-mail: danilo.tarquini@epfl.ch

[2]Research Associate, Earthquake Engineering and Structural Dynamics Laboratory, School of Architecture, Civil and Environmental Engineering, École Polytechnique Fédérale de Lausanne, EPFL ENAC IIC EESD, GC B2 484, Station 18, CH-1015 Lausanne, Switzerland. E-mail: joao.almeida@epfl.ch

[3]Associate Professor, Earthquake Engineering and Structural Dynamics Laboratory, School of Architecture, Civil and Environmental Engineering, École Polytechnique Fédérale de Lausanne, EPFL ENAC IIC EESD, GC B2 504, Station 18, CH-1015 Lausanne, Switzerland. E-mail: katrin.beyer@epfl.ch

Note. This manuscript was submitted on October 3, 2015; approved on March 23, 2017; published online on September 19, 2017. Discussion period open until February 19, 2018; separate discussions must be submitted for individual papers. This paper is part of the ***Journal of Structural Engineering***, © ASCE, ISSN 0733-9445.

Table 1. Lap Splice Strength Predicted according to Different Models

Test unit	Orangun et al. (1977)		Priestley et al. (1996)		Zuo and Darwin (2000)		Canbay and Frosch (2005)		Lettow and Eligehausen (2006)		COV (%)
	f_s (MPa)	$f_s > f_y$ (–)	f_s (MPa)	$f_s > f_y$ (–)	f_s (MPa)	$f_s > f_y$ (–)	f_s (MPa)	$f_s > f_y$ (–)	f_s (MPa)	$f_s > f_y$ (–)	
TW3	1,026	Yes[a]	987	Yes[a]	1,188	Yes[a]	669	Yes[a]	901	Yes[a]	17.8
VK2	774	Yes[a]	897	Yes[a]	700	Yes[a]	691	Yes[a]	627	Yes[a]	12.5
VK4	776	Yes[a]	900	Yes[a]	701	Yes[a]	692	Yes[a]	627	Yes[a]	12.6
VK5	736	Yes[a]	853	Yes[a]	678	Yes[a]	672	Yes[a]	611	Yes[a]	11.5
PW2	986	Yes[a]	838	Yes[a]	904	Yes[a]	1,159	Yes[a]	820	Yes[a]	13.1
RWS A-A	895	Yes[a]	844	Yes[a]	1,062	Yes[a]	815	Yes[a]	894	Yes[a]	9.5
RWS E-E	1,240	Yes[a]	1,092	Yes[a]	1,181	Yes[a]	1,189	Yes[a]	906	Yes[a]	10.5
W1/2	646	Yes[b]	714	Yes[a]	526	Yes[b]	544	Yes[b]	505	Yes[b]	13.6
CW2/3	343	No[c]	374	No[c]	428	No[c]	349	No[c]	393	No[c]	8.2
W-MC-60C	969	Yes[a]	891	Yes[a]	882	Yes[a]	968	Yes[a]	801	Yes[a]	6.9
W-MC-40C	681	Yes[a]	598	Yes[b]	645	Yes[b]	736	Yes[a]	655	Yes[b]	6.8
W-MC-60N	1,012	Yes[a]	930	Yes[a]	753	Yes[a]	817	Yes[a]	743	Yes[a]	12.3
W1*	277	No[c]	415	No[c]	393	No[c]	315	No[c]	480	Yes[b]	19.2
W2*	274	No[c]	409	No[c]	390	No[c]	313	No[c]	477	Yes[b]	19.3
Mean											12.4

Note: f_s = computed lap splice strength; f_u = measured rebar ultimate stress; f_y = measured rebar yield strength.
[a]$f_s > f_u$.
[b]$f_y < f_s < f_u$.
[c]$f_s < f_u$.

capacity. The latter was primarily addressed by means of plastic hinge models, for which moment-curvature relationships were adapted to account for the reduction in deformation capacity attributable to this constructional detail.

Existing FE simulations of the full monotonic or cyclic behavior of members with lap splices typically employ local bond-slip laws that have been developed for isolated anchored rebars, which is an effort in progress since the initial thriving phase of the FE method back in the late 1960s and early 1970s (Ngo and Scordelis 1967; Nilson 1972). Currently, the most well-known and widely employed model to describe the hysteretic response between bond stress and slip in an anchored bar failing by pull-out is the one proposed by Eligehausen et al. (1983). Cyclic bond-slip models for splitting failure (i.e., for bars with small concrete cover, such as in RC walls) are scarcer (ACI 2012), but a few recent proposals have addressed this gap (Harajli 2009; Harajli et al. 2004; Harajli and Mabsout 2002; Lowes et al. 2004).

Lap Splice Strength: Literature Review and Application to Wall Database

Several expressions have been proposed to compute the bond strength of spliced bars. Most of the available models aim at predicting the strength of single lap splices under monotonic loading and are based on estimations of an average bond stress. They were obtained either from regression analyses of experimental test data (Cairns 1985; Esfahani and Rangan 2000; Ichinose et al. 2004; Lettow and Eligehausen 2006; Orangun et al. 1977; Sozen and Moehle 1990; Zuo and Darwin 2000) or, more recently, using physically-based principles of tension cracking of concrete (Canbay and Frosch 2005; Priestley et al. 1996). Expressions derived from regression analysis of experimental tests under cyclic loading are also available in the literature, as those of Biskinis and Fardis (2010a) and Sakurada et al. (1993). In the following paragraphs, a qualitative overview of the previously discussed models is presented.

The first proposal for the strength of tension lap splices, based on a nonlinear regression analysis of results from beam tests under monotonic loading, is the one by Orangun et al. (1977). Their equation, which forms the basis for the bond requirements of the current ACI 318 Building Code (ACI 2011), reflects the effect of splice length, cover, spacing, bar diameter, concrete strength, and amount of transverse reinforcement on the strength of anchored bars. A similar expression for compression lap splices under monotonic axial loading was proposed by Cairns (1985). The parameters that influence the behavior of tensile lap splices play similar roles in compression splices but their relative importance changes. Namely, with respect to tension splices, the significance of transverse steel increases whereas the influence of concrete cover and bar size decreases. Sozen and Moehle (1990) proposed a simple lower-bound equation for the maximum tensile unit bond strength of anchored and spliced bars. Besides concrete cover, bar spacing, amount of transverse reinforcement, and concrete strength, the influence of casting position and epoxy-coated bars was also taken into account. More recently, Esfahani and Rangan (1998) also presented an expression for the estimation of the bond strength of tension lap splices for both normal and high-strength concrete. It was initially introduced for the unconfined case and later extended to account for transverse reinforcement (Esfahani and Rangan 2000). One of the most commonly used modeling approaches built on regression analysis of monotonic experimental data is the one provided by Zuo and Darwin (2000), which forms the basis for bond recommendations given by the ACI committee 408 (ACI 2003). The latter expresses the splice strength of bottom cast uncoated bars as a function of member geometry, concrete strength, relative rib area, bar size, and confinement exerted by both concrete and transverse reinforcement. An improvement of this model was proposed by Ichinose et al. (2004) whom, based on experimental data on pull-out and lap splice tests, modified the original equation to account for size effect. The revised expression suggests a large size effect for splices with small cover and short splice length—in which brittle failure is expected—and a small size effect for splices with low rib-height bars and high confinement—where ductile failure is likely. Based on a semi-empirical approach, an alternative formulation for the bond strength of spliced bars was proposed by Lettow and Eligehausen (2006) and included in the FIB model code (*fib* 2012). This category of methods consists in using numerical results from experimentally validated models to calibrate the proposed analytical equations.

To the authors' knowledge, there are only three models for lap splice strength currently available in the literature, based on statistical regression analyses, which are backed by an experimental database including cyclic loading tests, namely: the ones of Sakurada et al. (1993), Cho and Pincheira (2006), and Biskinis and Fardis (2010a). The first, using results from 16 beam specimens subjected to reversed cyclic loading tests, proposed an equation for the unit bond splitting strength depending on rebar diameter and spacing, amount of lateral reinforcement, and concrete strength. The second, using a database of 14 column tests under reversed cyclic loading, suggested a modification of the equation for lap splice strength available in FEMA 356 (U.S. Federal Emergency Management Agency 2000). Finally, the third built on a semi-empirical approach and arised from a large database composed of beams and columns. It proposes an expression in which the only parameters involved are the lap length, rebar diameter, and material strengths.

As discussed in the first paragraph of the present section, models with a theoretical mechanical basis were also developed. The first one, introduced by Priestley et al. (1996), estimates the strength of lap splices from considerations on the failure mechanisms and is applicable for circular and square beams and columns. The second, developed by Canbay and Frosch (2005), is built on a physical model of tension cracking of concrete in the lap-spliced region. Two different types of failure modes are considered: horizontal splitting that develops at the level of the bars (side-splitting failure), and vertical splitting that develops along the bar on the face cover (face-splitting failure). The resulting equation for the lap splice strength includes also a term that accounts for the presence of confining reinforcement, and it was validated against a database of beam tests with lap splices in constant moment regions loaded monotonically.

Table 1 lists the results in terms of lap splice strength, f_s, obtained by the application of the most relevant models among those previously described, to the database of RC walls with lap splices. The distinct models produce sensibly different results, with a mean and maximum coefficient of variation (COV) for the computed lap splice strengths of 12.4 and 19.3%, respectively. The table also compares the predicted values of f_s with the steel yield and ultimate stresses, f_y and f_u, respectively. When $f_s < f_y$, lap splice failure is expected before yielding of the longitudinal rebars. This feature should be accounted for in an equivalent steel stress-strain model for the characterization of lap splice behavior.

Deformation Capacity of Lap Splices

Although reliable estimations of the lap splice strength are required for structural assessment, the simulation of the available member ductility is no less important for seismic evaluation. When splices are short and unconfined, the yield strength of the lapped rebars cannot be achieved and premature failure is reached (Aboutaha et al. 1996; Chai et al. 1991; Melek and Wallace 2004; Valluvan et al. 1993). If an adequate lap splice length is adopted, the yield strength may be reached but a nonductile response is still expected if the level of confinement remains low (Paulay 1982). Further, in this situation, repeated cyclic loads above 75% of the yield strength may likely lead to failure (Lukose et al. 1982; Sparling and Rezansoff 1986). Finally, if splices are additionally well confined, not only the yield strength can be developed but also a degree of ductility is attainable (Gergely and White 1980; Lowes et al. 2012). Because splices primarily rely on force transfer by steel-concrete bond, which is an intrinsically brittle deformation mechanism that can be quickly exhausted, such displacement ductility capacity will be always lower than the ductility capacity of a continuous rebar, particularly under the effect of cyclic loads (Almeida et al. 2017). Nevertheless, for the assessment of existing structures such contribution to the inelastic deformation can be relevant and should not be neglected. It will be shown later that appreciable average strains at the onset of degradation, in the order of 3.5%, can be reached.

Plastic Hinge Models for Members with Lap Splices

Plastic hinge models are a common approach to predict the response of RC members. Several researchers have therefore proposed moment-curvature relationships to be used in conjunction with plastic hinge models that account for the presence of lap splices. Priestley et al. (1996) modify the moment-curvature relationship of members without lap splices as follows: firstly, it is checked whether the maximum equivalent tension stress in the rebar, derived from the computed lap splice strength, is less than the yield stress. In such case, a reduced moment capacity (M_s) is calculated, after which a postpeak branch begins. If the lap splice strength is sufficient to reach the nominal moment capacity (M_n), the latter is kept constant up to a curvature corresponding to a maximum fiber-compression strain $\varepsilon_c = 0.002$, which is then followed by a postpeak branch. The proposed softening branches for both cases are rather gradual, but the authors acknowledge the small database from which they were derived. The rationale behind the adoption of compression strain limits is related to the formation of longitudinal splitting cracks, which reduce the concrete resistance in compression and, consequently, in tension. Hannewald (2013), who also adopted compression strain limits in the context of plastic hinge analyses of three wall specimens with lap splices, observed that the previously indicated limit was a rather conservative bound. Instead, the strain at peak stress for confined concrete (ε_{cc}) suggested by Mander et al. (1988) was seen to provide better results, after which a sudden strength drop was assumed. A model accounting for tension failure of lap splices was proposed by Biskinis and Fardis (2007, 2010b), who suggested steel tensile strain limits for the outermost lap-spliced rebars. The strain limits were derived to fit the ultimate chord rotation (corresponding to a 20% drop in the member lateral resistance) as obtained from tests of columns and beams. Walls were not included in their database because most tests on walls with lap splices were carried out afterwards. The moment-curvature relationships of the previously discussed plastic hinge models accounting for the reduced deformation capacity of spliced RC members are qualitatively depicted in Fig. 1.

The estimation of the residual strength, intended as the force level that the lap splices can sustain without failing for large slip values, is a comparatively more challenging task, and there are no dependable conclusions on this point. Priestley et al. (1996) suggest to compute a residual moment (M_r) from the maximum eccentricity of the normal force within the core concrete, whereas other sources propose residual bond strengths ranging between 0 and 40% of the maximum strength, depending on the provided confinement (*fib* 2013). Following the experimental work by Bimschas (2010) and Hannewald et al. (2013), Hannewald (2013) stated that it does not seem reasonable to assume a slow cyclic strength degradation in between the onset of splice failure and a larger ductility at which the residual capacity is reached, unlike what other researchers had suggested (Biskinis and Fardis 2010b; Priestley et al. 1996).

FE Simulations of Members with Lap Splices

This section summarizes studies in which the behavior of RC members with lap splices was addressed with FE simulations. In

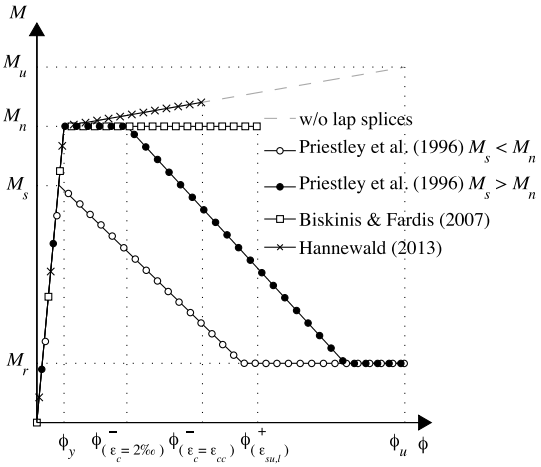

Fig. 1. Existing moment-curvature proposals for the evaluation of the deformation capacity of spliced RC members using plastic hinge models

this context, the use of frame lumped plasticity models for lap splice lengths larger than 25–30 diameters may be debatable because it becomes difficult to decide on the longitudinal reinforcement ratio to be assigned to the plastic hinge (i.e., single or double, see subsection on "Modeling Lap Splices as Double Reinforcement" for further details) and on the location of the plastic hinge at the wall base or above the spliced region. However, for short lap splices ($l_s < 25d_{bl}$), lumped plasticity models appear to be a valid modeling option. Rotational bond-slip springs combined with beam-column models have been used to simulate the response of column members (Cho and Pincheira 2006).

Xiao and Ma (1997) proposed a numerical model to obtain the monotonic force-displacement response of columns taking into account the deformation due to bond-slip in lap-spliced longitudinal rebars. It corresponds to a modified plastic hinge analysis wherein bond links are assumed for the lap splices above the hinge length, and it involves iterations to achieve equilibrium between bond and tensile force. A constitutive bond-slip law, based on a form of Popovics' equation (Popovics 1973) and accounting for the effects of confinement, is assigned to the links. The same relation was adopted by Binici and Mosalam (2007) to compute an effective steel stress taking into account bar slip, based on the assumption of a linear distribution of bond stresses along the lap splice length of both the starter and the spliced bar, and a decomposition of the total steel strain into slip strain and mechanical strain. These strain components are computed iteratively to satisfy equilibrium of stresses along the splice region and the bond stress-slip relationship. The same authors implemented the resulting model in a nonlinear analysis program with displacement-based frame elements with cross-sectional fiber discretization, which was later expanded to include cyclic lap splice behavior and a hysteretic damage component (Talaat and Mosalam 2008).

The concept of strain decomposition, together with idealized bond stress-slip relationships, was applied by other authors to develop truss elements (Kim et al. 2006, 2009) or bars with additional degrees of freedom to express the relative slip between steel and concrete (Girard and Bastien 2002). They were incorporated in refined FE models to simulate the response of columns with lap splices. Finally, Chowdhury and Orakcal (2012) included bond-slip behavior in a fiber-based flexural macromodel to simulate the cyclic response of RC columns with lap splices.

Detailed FE Models for Response of Walls with Lap Splices

Description of Nonlinear Shell Models

The 24 RC walls in the collected database were modeled using the nonlinear FE software *VecTor2* (*V2*) developed at the University of Toronto, which is based on the modified compression field theory (MCFT) (Vecchio and Collins 1986). All the defined models share the following features:

- Walls are modeled as cantilevers; an incremental lateral displacement Δ is imposed at the shear span height and, where present, a constant axial load N is applied simultaneously (push-over analysis). For the cases in which, due to the particular configuration of the test setup, the tested specimens represent only a portion of the actually imposed shear span (i.e., TW2, TW3, PW2, PW4, CW2, and CW3), a fictitious stiff collar is introduced to bridge the remaining part of the shear span up to the point of application of the imposed displacement.
- Foundation and top-loading beams belonging to the test setup were explicitly included in the models. Because no damage is expected in those regions, large tensile and compressive strengths ($\approx$100 MPa) were assigned to the corresponding concrete material. To achieve a realistic simulation of the confinement effect provided by the foundation to the wall, the concrete elastic stiffness was, however, not enhanced (which also helps promoting numerical convergence).
- Two different element types were employed for the structure discretization: plane stress rectangles and discrete truss bars. The former simulate the joint behavior of the concrete matrix and the horizontal reinforcement using a smeared approach. The latter model the longitudinal reinforcement and share the same nodes as the RC elements. For walls with lap splices, the effect of bond on the lap splice behavior was included by employing an equivalent stress-strain law in the truss elements of the lapped region; this model is derived in the next section. Such an implicit way of accounting for the bond-slip effect avoids the use of specific bond-slip elements (e.g., link or interface elements), which would simultaneously increase the computational demand and decrease the numerical stability of the analyses. Instead of using truss elements with perfect bond, the vertical reinforcement could have also been modeled as smeared reinforcement.
- Default *V2* settings concerning material models were adopted, which included: Hognestad (1955) and modified Park-Kent (Park et al. 1982) models for the prepeak and postpeak concrete in compression, respectively, and a linear elastic response before cracking with postcracking tensile stress equal to zero for concrete in tension. Strength and ductility enhancement due to confining reinforcement was calculated according to a combination of the models proposed by Kupfer et al. (1969) and Richart et al. (1928). The Mohr-Coulomb criterion is used to determine the failure shear stress, which is computed according to the MCFT (Vecchio and Collins 1986). For the reinforcing steel, the model proposed by Seckin (1982) including the Bauschinger effect is employed. The following modifications were made to the default models: (1) tension stiffening and softening were disregarded because their use showed to provide, for all RC walls, stiffer and stronger responses with respect to the experimental force-displacement curves—as also observed by Almeida et al. (2016); and (2) the model proposed by Palermo and Vecchio (2003, 2004) and suggested by Palermo and Vecchio (2007) and Pugh (2012) is used for the hysteretic behavior of the RC elements. Even when loaded monotonically up to failure,

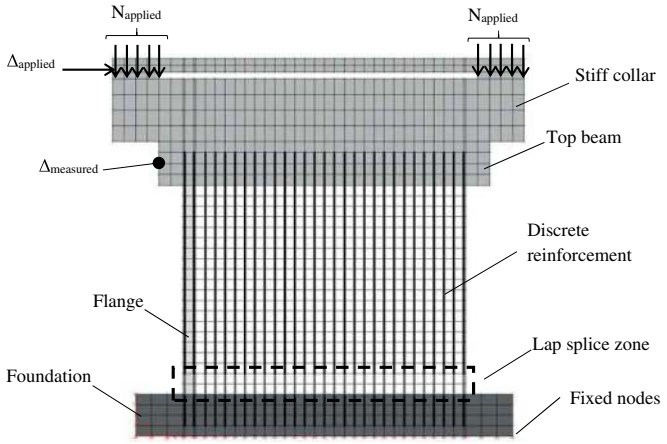

Fig. 2. Representation of shell and truss element mesh of wall TW3 using FE software *V2*

partial unloading and reloading occurs at the material level. It was observed that, when compared with simulations employing the default hysteretic model (Vecchio 1999), the model by Palermo and Vecchio (2003, 2004) leads to appreciable improvements in the global F-Δ results.

Fig. 2 displays as an example the mesh discretization of the specimen TW3 tested by the authors (Almeida et al. 2017). As noted, the displacement is applied at the wall cantilever height (i.e., at the shear span height) and does not necessarily correspond to the height of the displacement imposed in the experiment. The truss bar elements in the lap splice zone are depicted within a black dashed-line box in a lighter shade of grey; those are the elements to which the developed equivalent lap splice constitutive law will be assigned, as discussed later. For the entire set of test units, the material properties, geometrical features, and reinforcing layout are presented in Table 1 and Fig. 1 of Almeida et al. (2017).

Local-Level Validation of the Shell Element Model up to the Onset of Lap Splice Degradation

The FE model presented in this paper for the simulation of the force-displacement response of spliced RC walls builds on the definition of an equivalent constitutive model for the lap splice behavior up to the onset of structural strength degradation. The corresponding calibration requires information on local deformation quantities (namely vertical strains) from the collected database of members with lap splices. Due to the limited amount of available strain data (only 9 out of the 16 RC walls with lap splices were duly equipped to measure strains attributable to bond slip of lap splices), a semi-empirical approach was followed and the required local quantities were assembled as outcomes from advanced numerical models.

To justify the use of this approach, the reliability of the strain predictions originating from the FE models described in the previous subsection needs to be validated. To accomplish this goal, the vertical strains obtained from the numerical models are compared against the measured local experimental results from specimens TWs and VKs; the former were tested directly by the authors while the latter were tested partly by Bimschas (2010) and partly by Hannewald et al. (2013). In all these test series, experimental strains were derived from light-emitting diode (LED) measurements. For each couple of companion walls (i.e., TW2 versus TW3, VK1 versus VK2, VK3 versus VK4, and VK6 versus VK5), the comparison between numerical and experimental strains was carried out up to a level of displacement corresponding to the onset of strength degradation induced by the failure of the lap splices in the units that featured such constructional detail (i.e., TW3, VK2, VK4, and VK5). Beyond this displacement, softening of the force-displacement curve takes place, leading to complex phenomena of localized deformation. As the equivalent model proposed in this work is not intended to simulate this postpeak response range, the results beyond the onset of degradation are intentionally disregarded.

Fig. 3 shows the strain maps derived from experimental measurements for test units TW2 and TW3 at a lateral displacement level $\Delta = 16.5$ mm, which corresponds to the onset of strength degradation for wall TW3. The dimensions of the LED mesh employed to calculate the experimental strains were intentionally selected such that the bottom mesh layer included the main deformations resulting from bond slip occurring in the lap splice region (i.e., the horizontal cracks developing immediately above or below lap splices were considered as well). This choice was driven by the fact that finer meshes would depict strain concentrations where major cracks formed that cannot be numerically simulated by a model that accounts simultaneously for both mechanical and bond-slip straining. Only the positive loading direction (i.e., towards the flange side) is considered for this validation procedure because this is the direction where lap splices failed in tension. The observed vertical strain distributions in both test units (TW2 and TW3) are similar throughout the wall surface. Namely, in the element rows that include the lap splice region (i.e., the bottom layer), negligible differences in the order of 5% can be observed between the two test units. This latter remark is of relevance for the development of the proposed equivalent lap splice model.

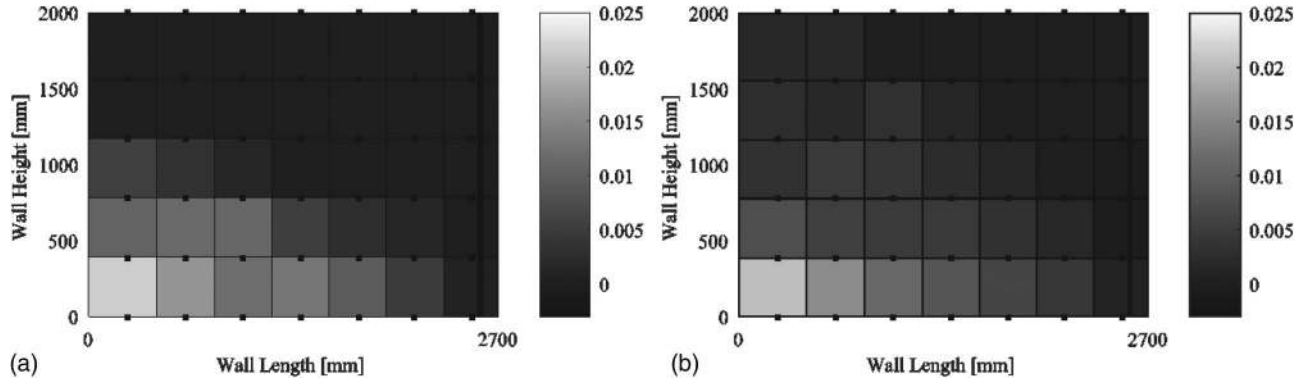

Fig. 3. Vertical strain map from experimental measurements at $\Delta = 16.5$ mm: (a) wall TW2; (b) wall TW3

J. Struct. Eng., 2017, 143(12): 04017157

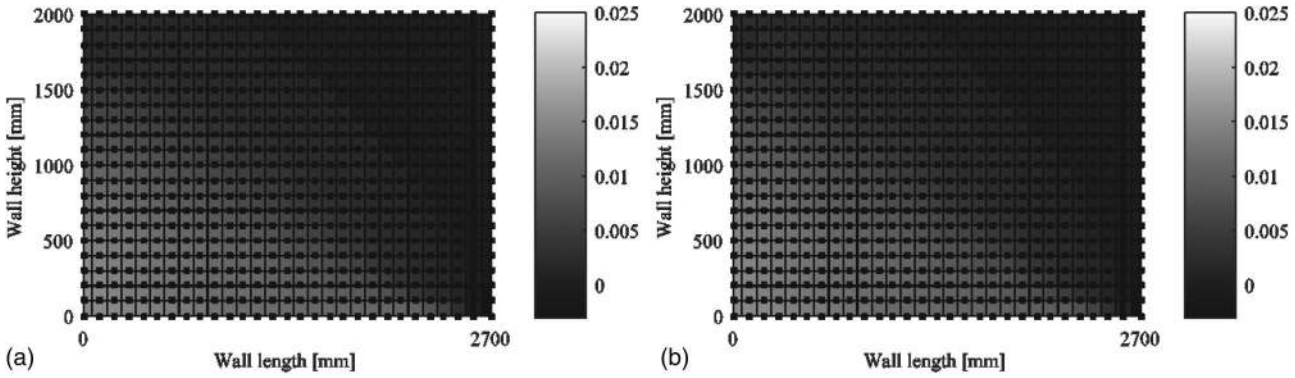

Fig. 4. Vertical strain map from numerical simulations at $\Delta = 16.5$ mm: (a) wall TW2; (b) wall TW3

The shell element model of walls TW2 and TW3, labelled *V2 cont. reinf.*, assumes continuous vertical reinforcement along the entire specimen height. This modeling choice does not account explicitly for the lap splices included in TW3. The hypothesis made by the authors in the present work and supported by the experimental evidences discussed in the previous paragraph (namely, comparable strain demands between TW2 and TW3) is that the behavior of a lap splice, until the onset of strength degradation, can be on average approximated by that of a single continuous rebar to which a regular stress-strain model is assigned. It is noted that, for the particular case of TW3, the computed lap splice strength f_s is larger than the yield strength f_y of the rebars (Table 1). For walls in which the splice strength is smaller than the rebar yield strength, such assumption is no longer valid and the proposed equivalent steel model will be adjusted accordingly in the next section. The strain distributions predicted by the shell element models at the same displacement level for which the experimental strains were evaluated, i.e., at the onset of splice strength degradation, are displayed in Fig. 4.

The strain distributions obtained from the FE models at the onset of degradation satisfactorily approximate the experimental ones observed for both walls TW2 and TW3 in Fig. 3. Almeida et al. (2016) showed that differences of the order of several hundred percent can be obtained in the evaluation of strain quantities in a RC member for different modeling techniques, even if based on the same material constitutive laws. The numerical models proposed in this paper, as shown later, yield relative errors in strain prediction that are consistently smaller than 50% in the plastic hinge zone, with an agreement that tends to improve for regions of the wall that remain in the elastic domain.

Observations on the experimental tests of the selected database indicate that the global strength degradation of RC walls is typically triggered by the tensile failure of the outermost layer of lap splices. The ability of the numerical model to simulate the previous finding was checked by averaging the vertical strains in the left corner membrane elements of the models of Fig. 4 along a mesh length similar to the one used for the experimental results shown in Fig. 3. The results in terms of relative error between the numerically predicted and the experimentally observed vertical strains for test units TW2 and TW3 are displayed in Figs. 5(b) and 6(b). This comparison was carried out for the displacement levels indicated in Figs. 5(a) and 6(a), which span from a nearly elastic response ($\Delta \approx 2$ mm) to the onset of wall strength degradation ($\Delta \approx 16.5$ mm). For both test units, the relative error in terms of vertical strains at the onset of strength degradation is approximately 30%. The average error along the entire displacement range up to strength degradation is of 40 and 20% for TW2 and TW3, respectively. In the next section ("Development of a Simplified

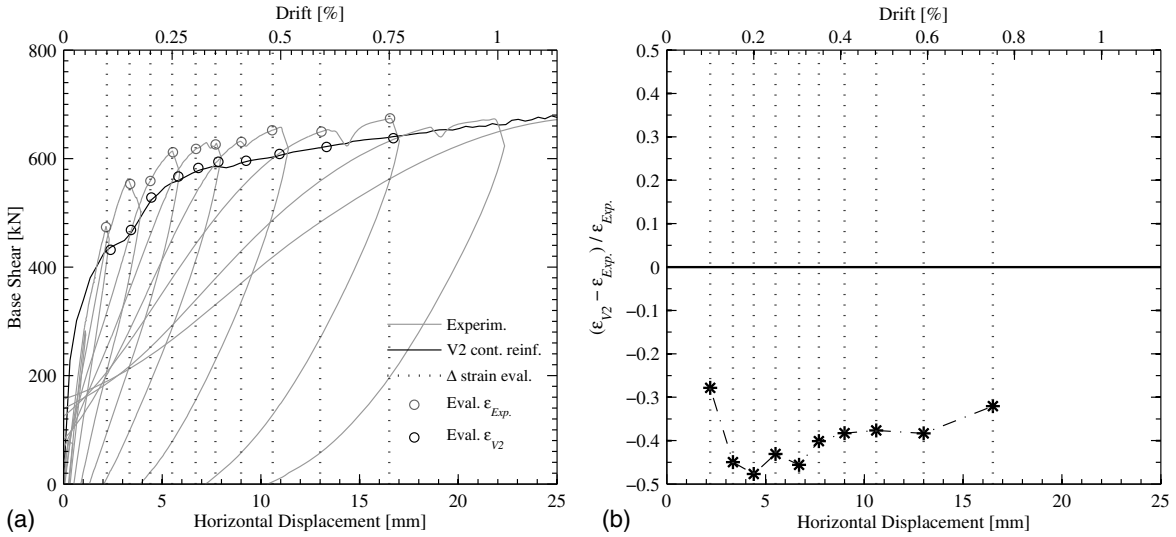

Fig. 5. Wall TW2: (a) points in the force-displacement curve at which the strains are evaluated; (b) relative error between experimental and numerical average strains at the outermost lap splice zone in tension

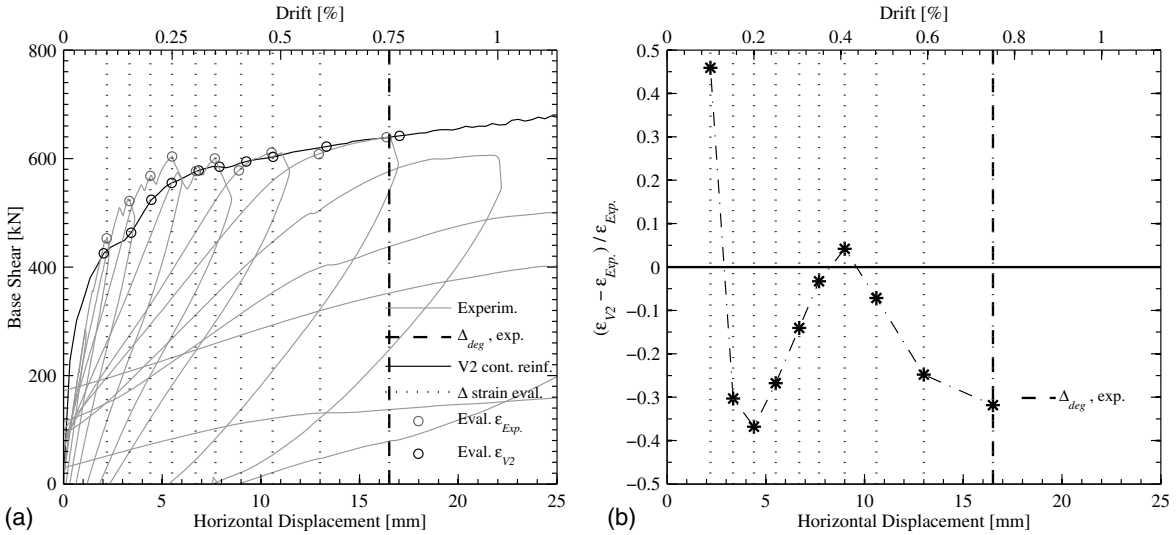

Fig. 6. Wall TW3: (a) points in the force-displacement curve at which the strains are evaluated; (b) relative error between experimental and numerical average strains at the outermost lap splice zone in tension

Constitutive Model for Lap Splices"), it is shown that such an error in strain prediction leads to errors in the displacement predictions of less than 20%. The good strain match in the elastic region of the wall explains the smaller errors obtained for member displacements.

To further validate the described FE model, the same comparative evaluation procedure was employed for the VK units as well, which were tested by Bimschas (2010) and Hannewald et al. (2013). Due to space limitations, the strain maps of the VK units are not herein included. Figs. 7(a and b) depict the relative error between experimental and numerical strains in the outmost lap splice region in tension for the reference units (VK1, VK3, and VK6) and the spliced units (VK2, VK4, and VK5), respectively. With the exception of VK4, for which the average relative error is approximately 45%, relative errors in vertical strains at the onset of degradation smaller than 20% were obtained. The ability of the employed nonlinear shell model in predicting vertical strains in the plastic zone can hence be considered dependable and will be used for the semi-empirical approach proposed in this paper.

Modeling Lap Splices as Double Reinforcement

When lap splices are long and well confined, the central region of both adjoining bars might be considered to effectively contribute to the lateral stiffness and resistance of the RC structural member. In such cases, doubling the flexural reinforcement in the lap splice zone could be considered to represent a legitimate modeling option.

A FE model with double reinforcement (labelled *V2 double reinf.*) was created, which is identical to the model *V2 cont. reinf.*, apart from the fact that the summed steel area of both spliced bars is assigned to the vertical reinforcing elements in the lap splice zone. The comparison in terms of force-displacement response between the experimental results and the models *V2 cont. reinf.* and *V2 double reinf.* is shown in Fig. 8 for three different RC walls, namely TW3, PW2, and W-60-C. The first one presents a uniform lap splice length of approximately 35 diameters without seismic confinement detailing while the remaining two test units exhibit code-compliant confined boundary elements with lap splice lengths of 48 and 60 diameters, respectively. As expected, doubling the

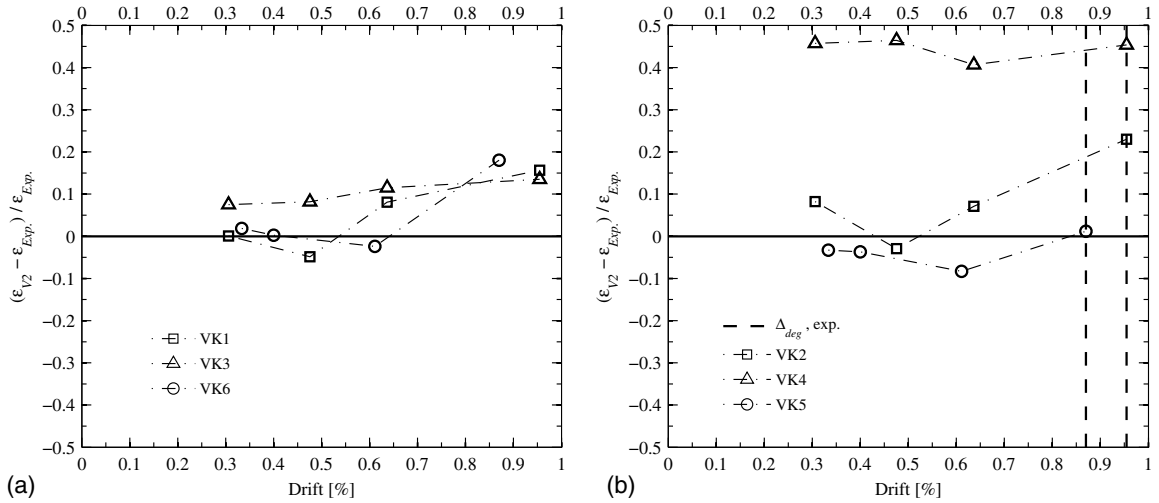

Fig. 7. Relative error between experimental and numerical average strains at the outermost lap splice zone in tension: (a) reference units VK1, VK3, and VK6; (b) walls with lap splices VK2, VK4, and VK5

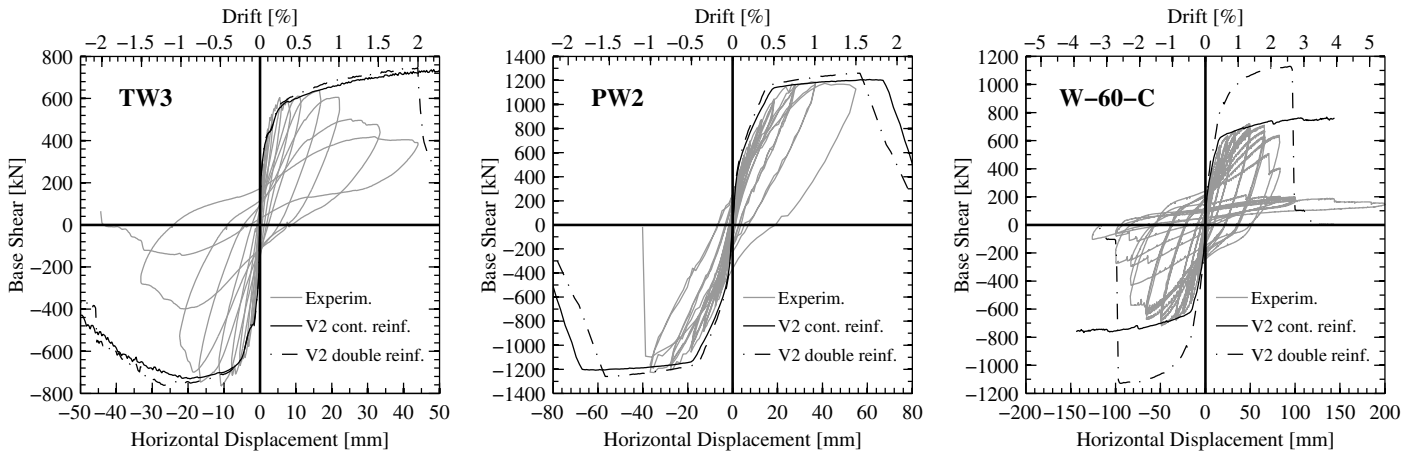

Fig. 8. Force-displacement curves of FE models with single and double reinforcement in the lap splice region

longitudinal reinforcement leads to larger predictions in terms of lateral strength and initial stiffness with respect to the model *V2 cont. reinf.* The latter provides a better match with the experimental results in the three cases. However, while for TW3 and PW2 the model *V2 double reinf.* still yields reasonable predictions at the global level, it overestimates the actual force capacity of W-60-C by a factor of approximately two. This can be explained as follows: when modeling lap splices with double reinforcement, the yielding of the flexural reinforcement may occur within or above the spliced region depending on the flexural demand-to-capacity ratio. If the flexural demand is approximately constant along the member length (i.e., low moment gradient), inelastic deformations will occur above the lap splice zone where single reinforcement is present, with a consequent reduction of the shear span. If, in contrast, there is a sharp moment gradient and the lap splice is long, it is possible that the demand within the double reinforcement region overcomes the capacity of the doubled rebars before the attainment of the single-bar capacity above the lap splice zone. The latter case is less common and did not occur in any of the wall models analyzed in this document. Whether the yielding of the flexural reinforcement above the spliced region has a significant effect on the global force-displacement response depends on the splice length to shear span ratio. TW3 and PW2 featured relatively small lap splice length to shear span ratios (6 and 9%, respectively). In contrast, the lap splice length to shear span ratio in W-60-C was larger than 40%; therefore, shifting the plastic section above the lap splice (which was not observed in the experimental test) increased the lateral strength considerably.

The numerical and experimental results were also compared at the local level for specimens TW3, VK2, VK4, and VK5. As an illustrative example, Fig. 9 shows the vertical strain map obtained with the model *V2 double reinf.* for wall TW3 at the onset of splice strength degradation. The doubling of the longitudinal reinforcing area causes vertical strains recorded in the lap splice zone to be considerably smaller than those obtained for the model *V2 cont. reinf.*, shown in Fig. 4(b). Considering that the spliced region of wall TW3 was not sufficiently long and confined to develop the strength of doubled continuous rebars, and recalling the use of perfect bond between concrete and steel in the models, an underestimation of the average lap splice vertical tensile strains (with consequent loss in accuracy) is expected when comparing numerical and experimental results. This is confirmed by contrasting Fig. 10(a) with its counterpart Fig. 6(b): the relative error in the strain prediction at the onset of degradation increases from approximately 30% for the model *V2 cont. reinf.* to 60% for the model *V2 double reinf.* The same reasoning applies for walls VKs where, in all cases, doubling the reinforcement worsens the strain predictions at the onset of degradation, compare Fig. 10(b) with Fig. 7(b). However, it should be acknowledged that for walls subjected to low moment gradient and featuring sufficiently long and well confined splices, the use of double reinforcement may turn out to be the best modeling option. Nonetheless, for the wall data set investigated in this study, modeling lap splices with double reinforcement leads to worse predictions of both global and local quantities.

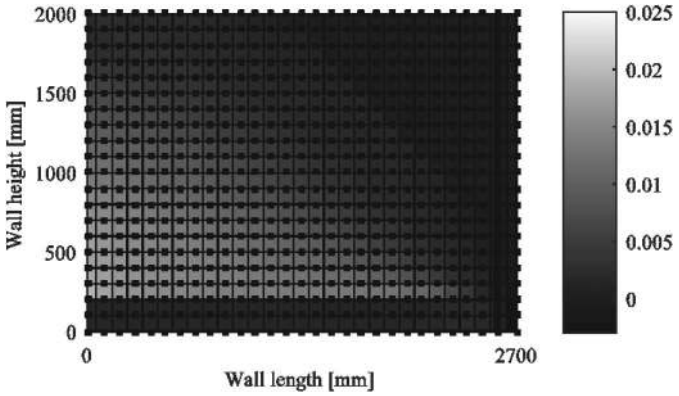

Fig. 9. Vertical strain map from numerical simulations for wall TW3 with double reinforcement in the lap splice region at $\Delta = 16.5$ mm

Development of a Simplified Constitutive Model for Lap Splices

Background and Assumptions for Development of Equivalent Uniaxial Steel Model

Although several studies can be found in the literature describing local bond-slip relationships under cyclic loading (Eligehausen et al. 1983; Harajli 2009; Harajli et al. 2004; Harajli and Mabsout 2002; Lowes et al. 2004), to the authors' knowledge no such relation is at present available for the global characterization of lap splice behavior. As a consequence, when FE methods are used to simulate the response of RC members featuring lap splices, the bond-slip contribution to the total deformation is normally

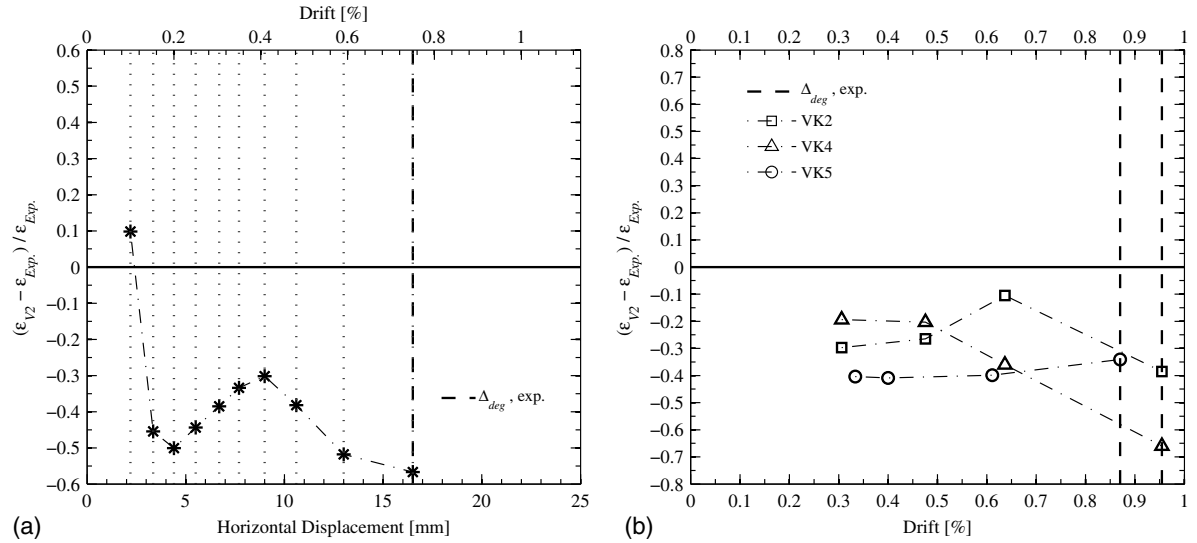

Fig. 10. Relative errors between experimental and numerical average strains at the outermost lap splice zone in tension using double reinforcement in the lap splice region: (a) wall TW3; (b) walls VK2, VK4, and VK5

accounted for in addition to the reinforcing steel straining component (through *ad hoc* bond-slip elements) and needs to be numerically integrated along the lap splice length. The complexity, both in terms of implementation and interpretation of the output, renders these models currently beyond usual engineering practice, also because bond-slip elements are often not implemented in commonly available software.

The main goal of this paper is to introduce a simple equivalent uniaxial stress-strain model capable of representing the combined behavior of the mechanically strained reinforcing steel and the bond-slip mechanism occurring within the lap splice. Such model should be conceptually similar to existing models available in common FE software and should be able to simulate with reasonable accuracy the detrimental effect of lap splices in the cyclic behavior of RC walls at the global level.

As a first remark, it is pointed out that the proposed equivalent average stress-average strain law for the splice element, although calibrated against cyclic tests on RC walls, is only applicable for monotonic loading, i.e., it will be a suitable tool for pushover analysis. However, because it was calibrated from data on cyclic tests, the effects of cyclic loading are indirectly included. The proposed stress-strain curve is composed of two parts (Fig. 11): an elastic branch, up to an equivalent yielding point ($\varepsilon_{y,ls}$, $f_{y,ls}$), and a postyield region up to an ultimate point ($\varepsilon_{u,ls}$, $f_{u,ls}$). The definition of these two points will be addressed in the following two subsections, which characterize the equivalent yield strength ($f_{y,ls}$) and the equivalent ultimate strain ($\varepsilon_{u,ls}$). The latter is set as the minimum between the tensile lap splice strain at the onset of structural member strength degradation, from now on identified as ε_{deg}, and the rebar fracture strain ε_{su}. Once these two quantities are determined, the corresponding counterparts (equivalent yield strain, $\varepsilon_{y,ls}$, and equivalent ultimate stress, $f_{u,ls}$) can be calculated straightforwardly. After the ultimate point, the equivalent stress is assumed to drop to zero. This simplifying hypothesis will naturally affect the global force-displacement response of the FE models, which will hence present an abrupt and conservative decay in strength capacity at the onset of lap splice degradation, shown later in Fig. 14. The following considerations support this assumption: (1) the

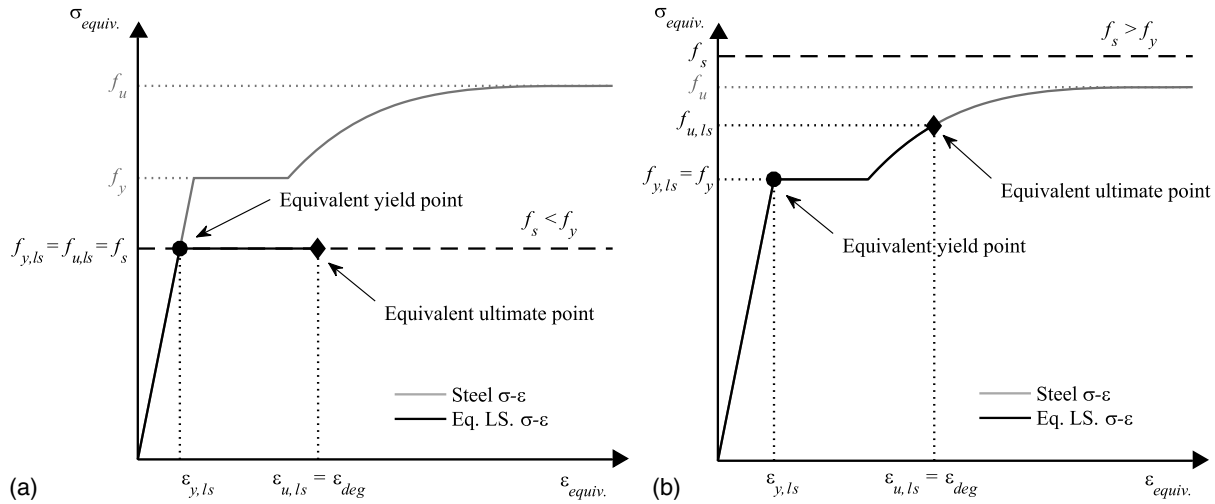

Fig. 11. Equivalent lap splice stress-strain law: (a) $f_s < f_y$; (b) $f_s > f_y$

experimental responses after the attainment of the peak force are highly unreliable and difficult to predict (this applies in particular to brittle deformation mechanisms such as those of lap splices, which are characterized by steep softening slopes); and (2) from the numerical point of view, localization phenomena come into play rendering the outcomes of nonlinear FE analysis untrustworthy and mesh dependent (Almeida et al. 2016; Calabrese et al. 2010).

Lap Splice Strength

The equivalent yield point is defined by the equivalent yield stress ($f_{y,ls}$) and the equivalent yield strain ($\varepsilon_{y,ls}$), which is simply obtained dividing the former by the Young's modulus E_s of the reinforcing steel (Fig. 11). It is thus assumed that, up to the equivalent yield point, the lap splice element acts as a single embedded continuous rebar.

The equivalent yield stress $f_{y,ls}$ is determined as the minimum between the steel yield stress f_y and the lap splice strength f_s. In short and poorly detailed splices, the spliced rebars will not reach the yield strength. As soon as the first splitting crack forms and the surrounding concrete begins to loosen its clamping action, most of the lap splice deformation will come from relative bar slippage. No further stresses will thus accumulate in the spliced bars resulting in a diminished overall force capacity. This observation finds support in the comparison between experimental and numerical results (shown later in Fig. 14): for those walls featuring a splice strength f_s smaller than the steel yield strength f_y, the results obtained from the FE model employing continuous vertical reinforcement (*V2 cont. reinf.*) lead to a considerable overestimation of the experimental member strength capacity. In contrast, for well detailed lap splices (i.e., with adequate splice length and confining reinforcement) the concrete matrix surrounding the adjoining bars will be able to transfer entirely the stress at yielding of the single rebar.

The model proposed by Canbay and Frosch (2005) was chosen among the available formulations to compute the splice strength f_s for the following two reasons: (1) it is the most recent and more advanced within the available physical-based approaches, explicitly accounting for different lap splice failures, namely side- and face-splitting; and (2) due to the theoretical framework on which Canbay and Frosch's model (2005) builds on, it is more suitable than statistical approaches to be extended outside the member data set forming the domain of validation, which include RC beams and columns.

In the context of the present work, the main limitations of the expression proposed by Canbay and Frosch (2005) are: (1) it was derived for strength evaluation of tension splices under monotonic loading; and (2) it does not account for the beneficial effect of the moment gradient on lap splice strength. Following the discussion in the companion paper (Almeida et al. 2017), monotonic splice strength is in this paper accepted as an estimate of the splice capacity under cyclic loading.

Strain at Onset of Strength Degradation

A pivotal point in the definition of the equivalent stress-strain relationship for lap splices in RC walls is the identification of the ultimate strain limit $\varepsilon_{u,ls}$, which is defined as the minimum between the strain at the onset of strength degradation ε_{deg}, and the rebar fracture strain ε_{su}. To the authors' knowledge, few propositions are currently available in the literature to determine analytically the lap splice strain capacity. Moreover, as already pointed out, they are all targeted at application with plastic hinge methods. The next paragraphs develop an estimate of the strain at the onset of degradation by means of a semi-empirical approach.

Firstly, the RC walls with lap splices included in the assembled database were modeled with the nonlinear FE software *V2* as discussed in the previous section. Exception was made for specimens PW2 and RWS, which were disregarded for the following reasons: the first did not show any sign of strength degradation due to lap splices while the second, featuring four different types of longitudinal rebars and splice lengths, depicted a cyclic behavior that was not amenable to be analytically simulated. A similar argument holds with respect to the companion unit with continuous longitudinal reinforcement, RWN. Single reinforcement is used along the entire height of the test units because, as previously remarked, this represents the best available modeling option both in terms of global and local level results. It is noted that, for those cases in which the lap splice strength f_s is smaller than the steel yield stress f_y, an elastoplastic stress-strain law was assigned to all the reinforcing truss elements simulating the lap splices. The latter is described in the next section representing the basis for the model $V2w/f_s$.

Secondly, the maximum vertical tensile strains of the outermost steel elements located in the lap splice region are recorded for three different displacements: at the onset of strength degradation as observed from the experimental tests (Δ_{deg}), and at a lower and upper bound of this value in a 20% interval ($\Delta_{\text{LB}} = \Delta_{\text{deg}} - 0.2 \times \Delta_{\text{deg}}$; $\Delta_{\text{UB}} = \Delta_{\text{deg}} + 0.2 \times \Delta_{\text{deg}}$). This procedure allows to obtain a range of variation for the strains around the onset of strength degradation, which are then useful to calibrate the predictive equation. The choice of considering the most strained lap splice in tension reflects the fact that, in all the selected experimental studies on RC walls with lap splices, failure of the outermost layer of lap splices signals a marked specimen strength degradation (Almeida et al. 2017). The maximum value of the vertical steel strain along the lap splice was monitored because of the following considerations: (1) in the case of short splices, or long splices under small moment gradient, the strain distribution is rather constant along the splice length; and (2) for long splices under high moment gradient, strength degradation can start without splitting cracks developing along the entire splice length, especially if the lap splice is not well confined. The use of an average strain value along the splice length would thus lead to nonconservative estimates of the strain at strength degradation.

The results obtained for the strain at degradation onset $\varepsilon_{V2(\Delta\,\text{deg})}$ are listed in Table 2 together with its lower and upper bounds, $\varepsilon_{V2(\Delta\text{LB})}$ and $\varepsilon_{V2(\Delta\text{UB})}$, respectively. The relative errors between these quantities and $\varepsilon_{V2(\Delta\,\text{deg})}$ are also included in the table and it can be observed that they are on average larger than the error arising from the strain estimation by the employed refined FE model (approximately 30%, as shown in the previous section). The latter can therefore be considered to provide dependable results and the use of the semi-empirical approach is thus justified.

Before introducing the proposed equation for the strain at the onset of degradation, the method used to select the governing parameters is described. Firstly, an initial set of parameters deemed potentially relevant for the strain capacity of lap splices was singled out. Subsequently, their correlation with the strain at the onset of degradation was assessed through univariate regression analyses. Finally, the coefficient of determination was computed for each parameter, allowing to identify the most important ones, as discussed next.

Transverse (confining) reinforcement is undoubtedly the most critical factor controlling the strain at degradation onset because it enables the force transfer mechanism between spliced bars once splitting cracks have formed and because it allows for a more effective yield penetration, which prevents sudden strength

Table 2. Strains at the Onset of Degradation with Associated Lower and Upper Bounds, Values Estimated with Eq. (1), and Comparison

RC wall	$\varepsilon_{V2(\Delta\,\mathrm{deg})}$ (‰)	$\varepsilon_{V2(\Delta\mathrm{LB})}$ (‰)	$\varepsilon_{V2(\Delta\mathrm{UB})}$ (‰)	$\frac{\varepsilon_{V2(\Delta\mathrm{LB})}-\varepsilon_{V2(\Delta\,\mathrm{deg})}}{\varepsilon_{V2(\Delta\,\mathrm{deg})}}$ (%)	$\frac{\varepsilon_{V2(\Delta\mathrm{UB})}-\varepsilon_{V2(\Delta\,\mathrm{deg})}}{\varepsilon_{V2(\Delta\,\mathrm{deg})}}$ (%)	$\varepsilon_{\mathrm{deg}}$ (‰)	$\frac{\varepsilon_{\mathrm{deg}}}{\varepsilon_{V2(\Delta\,\mathrm{deg})}}$
TW3	14.73	11.25	18.46	−24	25	13.44	0.912
VK2	18.81	10.39	31.75	−45	69	10.86	0.577
VK4	10.29	6.01	20.88	−42	103	10.86	1.055
VK5	6.64	4.01	10.69	−40	61	9.40	1.416
W1	11.94	10.74	14.14	−10	18	13.88	1.163
W2	14.25	12.18	17.10	−15	20	12.77	0.896
CW2	3.78	1.82	4.90	−52	30	3.90	1.032
CW3	6.46	3.20	9.85	−51	52	6.54	1.013
MC-60-C	30.31	25.30	35.40	−17	17	34.03	1.123
MC-40-C	29.69	24.63	35.85	−17	21	29.93	1.008
MC-60-N	24.62	20.17	27.07	−18	10	26.00	1.056
MC-60-N2	25.46	19.37	28.51	−24	12	26.04	1.023
W1-L	8.33	3.39	13.18	−59	58	7.11	0.854
W2-L	7.59	2.57	13.50	−66	78	7.10	0.936
Mean	—	—	—	34	41	—	1.005
SD	—	—	—	—	—	—	0.178

degradation. Lap splice length, shear span (which accounts for the moment gradient), and loading history are the other fundamental quantities governing the lap splice deformation behavior. Due to the difficulty in evaluating the effects of the loading history, they are only indirectly taken into account in the expression for the splice strain capacity in the measure that the RC walls in the database were subjected to cyclic loading histories.

Once identified the previously discussed fundamental quantities, a final multivariate regression analysis yielded the following expression for $\varepsilon_{\mathrm{deg}}$, valid for RC walls with mechanical and geometrical features within the range of the walls in the database

$$\varepsilon_{\mathrm{deg}} = \varepsilon_{y,ls} + 0.65 \cdot \rho_w + 0.03 \cdot \frac{l_s}{L_s} \tag{1}$$

where $\varepsilon_{y,ls}$ = equivalent yield strain; l_s = length of the outermost lap splice in tension; L_s = shear span of the member; and ρ_w = confining reinforcement ratio defined as

$$\rho_w = \rho_x + \rho_y \tag{2}$$

$$\rho_x = A_{\mathrm{trx}} \cdot \frac{n_{\mathrm{legs}}}{s_x \cdot b} \tag{3}$$

$$\rho_y = \frac{A_{\mathrm{try}}}{s_y \cdot (d_{bl} + c_{b0})} \tag{4}$$

where ρ_x and ρ_y = reinforcement ratios in the plane parallel and orthogonal to the plane of bending; A_{tr} = area of the confining stirrups; s = spacing; n_{legs} = number of stirrup legs; d_{bl} = diameter of the longitudinal bars; b = section width; and c_{b0} = clear face concrete cover.

It is important to point out that, if the transverse reinforcement cannot exert its confining action, either because there are no stirrups or because the shear reinforcement is not appropriately detailed at the wall edges (135° hooks or closed up), the value of ρ_w should be set equal to zero. In such cases, when the splitting cracks form, no additional force transfer mechanism between adjoining rebars is possible and strength degradation due to bond slip will occur. Within the assembled database of RC walls, this is the case of specimens CW2, CW3, W1*, and W2*, tested by Elnady (2008) and Layssi and Mitchell (2012).

The influence of the parameters ρ_w and l_s/L_s on the strain at the onset of degradation $\varepsilon_{V2(\Delta\,\mathrm{deg})}$ is presented in Figs. 12(a and b), evidencing strong correlation. The last two columns of Table 2 report the strains at the onset of degradation computed with Eq. (1), referred to as $\varepsilon_{\mathrm{deg}}$, and the ratio with respect to those from the nonlinear FE analyses, $\varepsilon_{V2(\Delta\,\mathrm{deg})}$. The estimated values are very close to the ones given by the numerical model, with an average ratio $\varepsilon_{\mathrm{deg}}/\varepsilon_{V2(\Delta\,\mathrm{deg})}$ close to unity and a coefficient of variation smaller than 20%. In Fig. 13, the goodness of fit of the estimated strains is represented in the form of an error-bar plot. In all cases, the values of $\varepsilon_{\mathrm{deg}}$ fall within the range of variation of $\varepsilon_{V2(\Delta\,\mathrm{deg})}$, represented by the interval $[\varepsilon_{V2(\Delta\mathrm{LB})}, \varepsilon_{V2(\Delta\mathrm{UB})}]$ and the prediction is, therefore, judged satisfactory.

Once the strain at the onset of degradation $\varepsilon_{\mathrm{deg}}$ is estimated with Eq. (1), which corresponds to the ultimate strain $\varepsilon_{u,ls}$ of the proposed equivalent lap splice constitutive law, the equivalent ultimate stress $f_{u,ls}$ can be determined accordingly (Fig. 11):

- If the steel yield stress f_y is larger than the lap splice strength f_s, i.e., when $f_{y,ls} = f_s$: an elastic perfectly plastic stress-strain curve is assumed for the equivalent steel and, hence, $f_{u,ls} = f_{y,ls} = f_s$. Strains beyond $f_{y,ls}$ come from bond slip and not from mechanical straining of the rebar.
- If the steel yield stress f_y is smaller than the lap splice strength f_s, i.e., when $f_{y,ls} = f_y$: the stress-strain curve of the equivalent uniaxial material is assumed to be equal to the reinforcing steel's up to the value of $\varepsilon_{u,ls}$. Hence, when present, the yield plateau or hardening branch of the steel constitutive law should be considered. In the particular case where $f_y < f_s < f_u$, it is possible to obtain an equivalent ultimate stress $f_{u,ls}$ larger than the estimated lap splice strength f_s. However, the authors believe that, due to the unavoidable inaccuracy related to the evaluation of the lap splice strength f_s, a separate consideration of this scenario is not justified; additionally, the latter is very uncommon and did not occur for any of the spliced walls included in the assembled database.

Validation of Model against Wall Database

Fig. 14 shows the comparison between the experimentally measured force-displacement curves and the numerical simulations for all the RC walls in the database, which includes 16 specimens with lap splices and 8 with continuous reinforcement. The walls with continuous reinforcement along the entire height represent the reference units for 10 of the walls with spliced bars and are included for two main reasons: they serve as benchmark for the numerical models

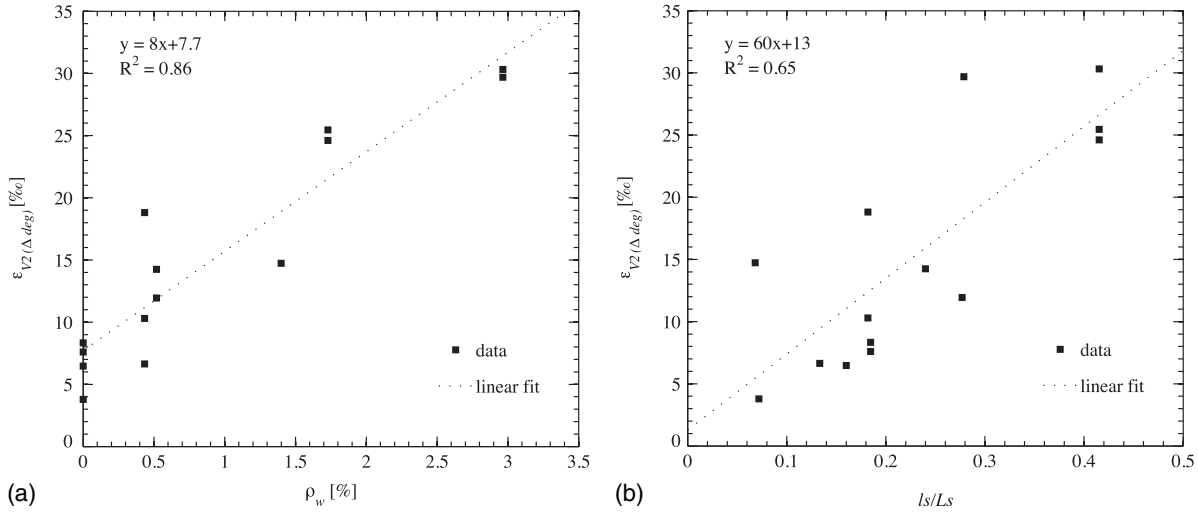

Fig. 12. Strain at degradation onset simulated by the *V2* models versus (a) reinforcement ratio ρ_w; (b) ratio between the lap splice length and the shear span l_s/L_s

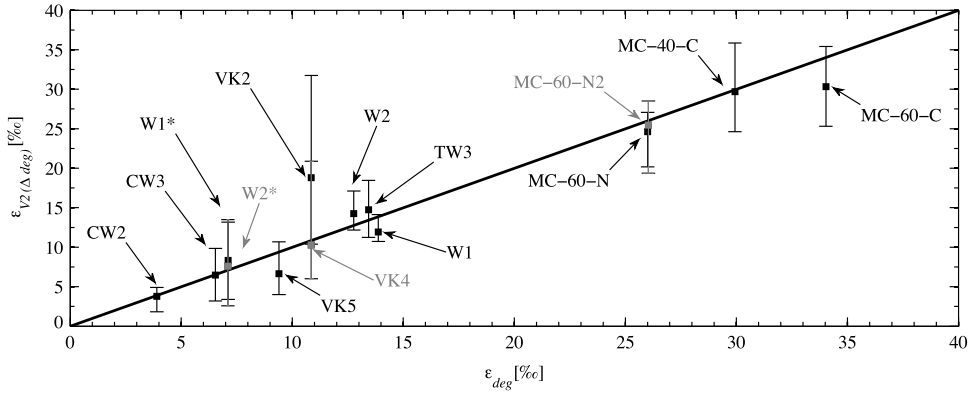

Fig. 13. Comparison between strains simulated by *V2* and those estimated with newly proposed Eq. (1)

(e.g., if the FE model is not able to accurately predict the response of the reference wall, then the simulation results obtained for the companion spliced wall cannot be considered as reliable), and they put into evidence the premature failure of walls with lap splices.

The employed shell element models were developed with the nonlinear FE software *V2* (their common features were listed in the subsection "Description of Nonlinear Shell Models") and are described as follows:

- Model with continuous reinforcement (*V2 cont. reinf.*): the vertical (flexural) reinforcement is modeled as continuous throughout the entire height of the wall specimen. Although this is an appropriate approach for the reference unit walls, it does not account for the presence of lap splices.
- Model accounting for lap splice strength (*V2* w/f_s): for all bar elements representing the longitudinal reinforcement in the lap splice zone, an equivalent elastoplastic constitutive law accounting for the maximum splice bond strength f_s is used. The equivalent steel yield stress is set equal to the lap splice strength f_s as computed according to the model by Canbay and Frosch (2005). A large value (> 10%) is imposed for the equivalent steel ultimate strain. The purpose of this model is to show the reduction in the numerically predicted capacity of the test units in which a prior-to-yielding lap splice failure was expected (i.e., walls W1, W2, CW2, and CW3 in the authors' database).
- Proposed model (*V2* $w/eq.$ *LS*): the uniaxial average stress-average strain law described in the previous section (Fig. 11) is assigned to all the vertical steel elements within the lap splice zone. This model accounts for the limited lap splice strength and strain capacity.

In the plots of Fig. 14, horizontal displacements and drifts are indicated on the primary and secondary x-axis, respectively. Except for the walls tested as cantilevers, the reported displacements do not necessarily correspond to the ones imposed in the pushover analyses. If a particular test setup is used to impose a bending moment at the top of the specimen (as for walls TW2, TW3, PW2, PW4, CW2, and CW3), the plotted displacements are those experimentally measured at the point of application of the lateral load. The lateral drift is calculated as the ratio between the measured displacements and the height above the foundation at which the measurement is taken. The base shear is shown on the y-axis. To ease the interpretation of the results, a dashed line displays the experimentally observed displacement at the onset of strength degradation (Δ_{deg}). In the following paragraphs, the obtained results with each of these models are discussed and compared.

The reference unit walls are discussed first. Up to the peak force of the experimental results, the FE model with continuous reinforcement is able to accurately predict the backbone curve of the cyclic responses. The only exception is given by wall RWN where, for

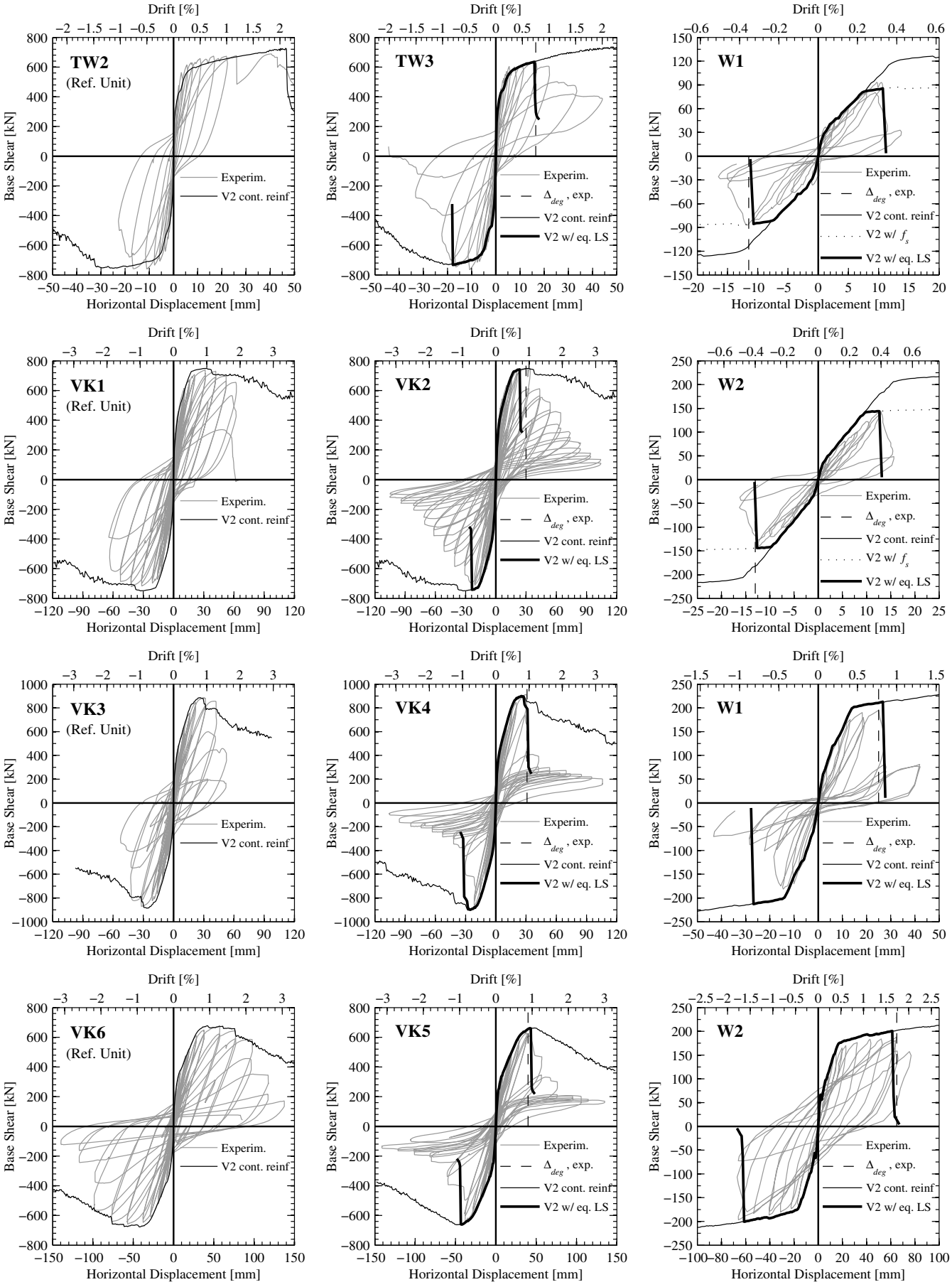

Fig. 14. Comparison between force-displacement curves obtained experimentally and numerically

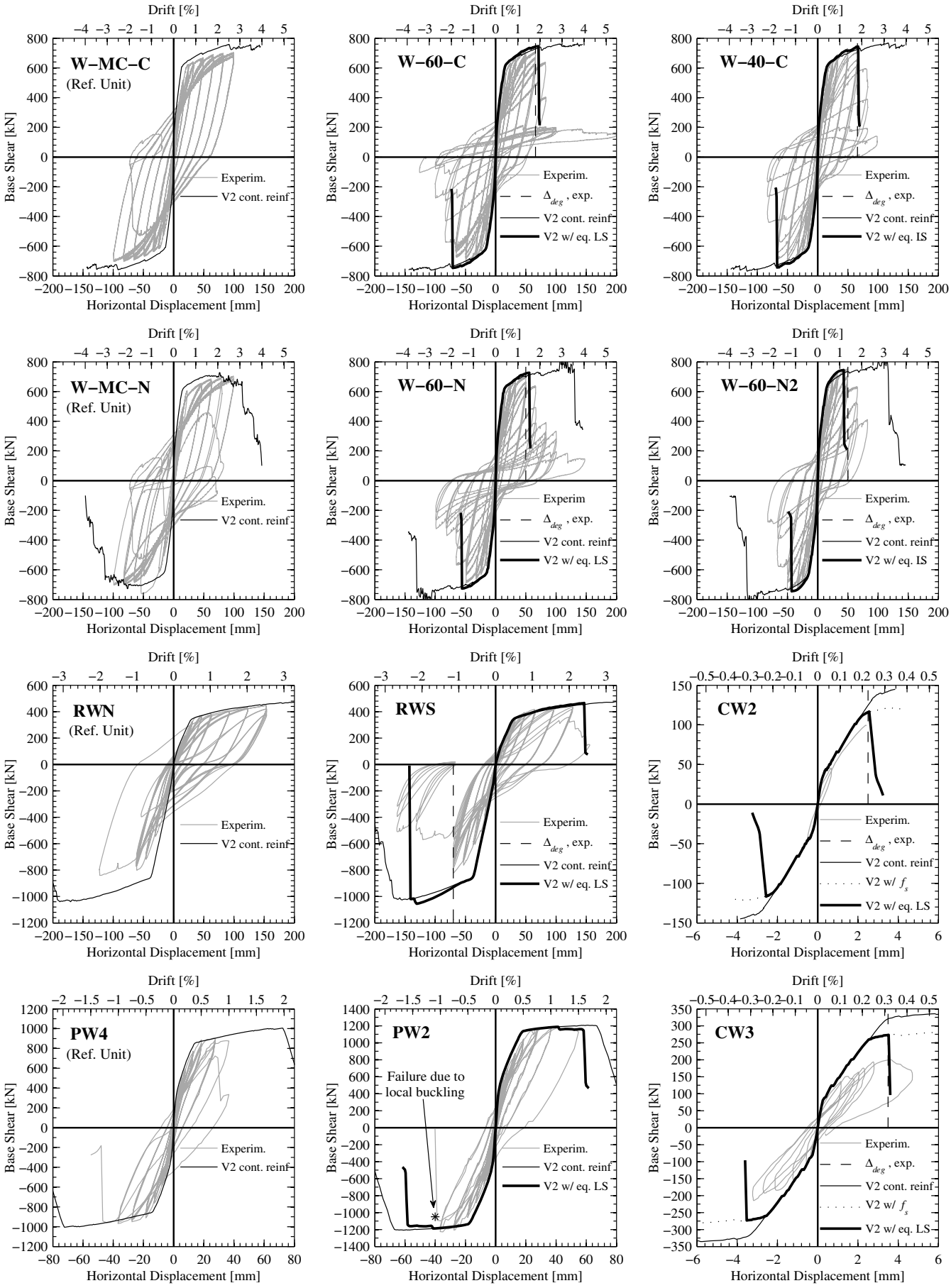

Fig. 14. (*Continued.*)

negative drift values, the postelastic stiffness degradation and the maximum force capacity are not well captured. The nonsymmetrical layout of the flexural reinforcement presented by this specimen, leading to a complex cyclic behavior, can contribute to explain why the model fails to effectively simulate the experimental results. However, the analytical monotonic response is close to the one shown by the authors of the test (Aaleti et al. 2013), obtained with a plastic hinge model. Regarding the displacement at which the peak force is attained, the numerical simulations provided noticeably good results as well. An exception is again the wall RWN but also PW4, for which the previously discussed displacement level is considerably overestimated. Beyond the displacement at peak force the model response is subjected to numerical pathologies and it should not be considered as dependable. Therefore, no discussion will follow on the comparison between the numerical and experimental postpeak responses.

The presence of lap splices in the region of RC walls in which inelastic deformations are expected can lead to two detrimental effects: (1) reduction in the force capacity of the structural member; and (2) anticipation of the process of strength degradation due to bond deterioration occurring between adjoining bars. The first scenario is expected when the splice strength is not sufficient to transfer the rebar yielding force. In the selected database, and according to the chosen equation for the splice strength (Canbay and Frosch 2005), this occurred in only four cases, namely specimens W1, W2, CW2, and CW3. For those test units, the model with continuous reinforcement largely overestimates the experimental force capacity. A better estimate of the latter is obtained by employing the model $V2w/f_s$ represented in the plots of Fig. 14 with a dotted line. As it is shown, the maximum base shear predicted by this model is in line with the experimental results for walls W1, W2 and CW2, although for CW3 it overestimates the experimental results by almost 40%. The use of a smaller value of f_s with respect to Canbay and Frosch's proposal (Canbay and Frosch 2005) in the equivalent constitutive law of wall CW3 would improve the predicted force capacity. However, none of the modeling approaches available in the literature provided a sufficiently low estimate of the splice strength (Table 1).

The effect of lap splices on the displacement capacity of RC walls is not captured by any of the previously discussed models, i.e., neither *V2 cont. reinf.* nor *V2 w/fs*. However, for almost all the test units featuring lap splices, the model *V2 w/eq. LS* correctly identifies the displacement at the onset of structural strength degradation caused by the lap splices' detrimental effect (Δ_{deg}). The only exception is represented by the wall RWS, where Δ_{deg} is overestimated. A particular case is also PW2, which, although featuring lap splices, did not show any evident sign of strength degradation. Rather, the specimen failed due to local buckling of the vertical rebars above the lap splice zone of the boundary elements. For this case Eq. (1) predicts a lap splice strain capacity of 3%, which is larger than the numerical strain recorded in the outermost rebar in tension at the ultimate displacement level hence consistent with the experimental results. Looking at the overall shape of the force-displacement curves obtained with the model *V2 w/eq. LS*, one can notice the presence of a sudden drop in force at the level of the ultimate displacement. This does not come as a surprise and corresponds to the attainment of the ultimate equivalent strain $\varepsilon_{u,ls}$ in the longitudinal reinforcing elements within the lap splice zone. A residual strength to the modified steel constitutive law would have to be assigned to obtain a global gradually descending branch. Further research would be required to dependably use the latter approach and to deal with the consequent numerical problems such as localization.

A final remark is due on the fact that the same database of RC walls is used for the validation procedure and for the determination of the equivalent uniaxial lap splice stress-strain law. As a consequence, a good agreement between the analytical (model *V2 w/eq. LS*) and experimental results could, in principle, be expected. The reason behind the use of the same database lies in the limited number of spliced RC walls that are available in the literature. One alternative could have been to split the data set in two parts and use one for calibration and another for validation. The authors investigated such an approach by performing a robustness analysis. The parameters of the predictive equation were determined with any combination of 8, 10, or 12 specimens out of the 14 test units with lap splices, showing a robust fit. The entire set of walls naturally provided the best match, from which the predictive equation was derived.

Conclusions

Lap splices are frequently found at the wall base of existing RC structures and recent ones that are not designed for a ductile response. The simulation of the behavior of lap splices is a challenging task, as it is affected by many factors, the influence of which is mostly understood only from a qualitative viewpoint. This contrasts with the engineering need to have a simple but dependable model to account for lap splice response. This paper proposes an equivalent uniaxial steel stress-strain model that represents the monotonic envelope of the cyclic response of lap-spliced rebars up to the onset of strength degradation. It is characterized by two points defining an equivalent yield state and an ultimate condition. A new expression is introduced to estimate lap splice strain capacity, which was calibrated from a semi-empirical approach. It depends on the equivalent yield strain, confining reinforcement ratio, and ratio of lap splice length to shear span, which turned out to be the parameters mostly influencing the ductility capacity of lap splices. The derived expression shows an average ratio of predicted versus semi-empirical strains close to unity and a mean coefficient of variation below 20%. The newly proposed equivalent steel stress-strain model was used in combination with nonlinear shell element models to simulate the response of all the RC walls in the database, showing a good accuracy in the evaluation of both member strength and displacement capacity. Beyond the point of strength degradation the prediction of member lateral resistance becomes nondependable and hence was not addressed.

Acknowledgments

The financial support by the *Stiftung zur Förderung der Denkmalpflege* of the project "Erbebenverhalten von bestehenden Stahlbetongebäuden mit dünnen Wänden" and by the *Swiss Federal Roads Office (FEDRO)* to the project number AGB 2015/002, under which the present study was partly carried out, are acknowledged.

References

Aaleti, S., Brueggen, B. L., Johnson, B., French, C. E., and Sritharan, S. (2013). "Cyclic response of reinforced concrete walls with different anchorage details: Experimental investigation." *J. Struct. Eng.*, 10.1061/(ASCE)ST.1943-541X.0000732, 1181–1191.

Aboutaha, R. S., Engelhardt, M. U., Jirsa, J. O., and Kreger, M. F. (1996). "Retrofit of concrete columns with inadequate lap splices by the use of rectangular steel jackets." *Earthquake Spectra*, 12(4), 693–714.

ACI (American Concrete Institute). (2003). "Bond and development of straight reinforcing bars in tension." *ACI 408R-03*, Farmington Hills, MI.
ACI (American Concrete Institute). (2011). "Building code requirements for structural concrete." *ACI 318M–11*, Farmington Hills, MI.
ACI (American Concrete Institute). (2012). "Report on bond of steel reinforcing bars under cyclic loads." *Joint ACI-ASCE Committee 408*, Farmington Hills, MI.
Almeida, J. P., Prodan, O., Tarquini, D., and Beyer, K. (2017). "Influence of lap-splices on the cyclic inelastic response of reinforced concrete walls. I: Database assembly, recent experimental data, and findings for model development." *J. Struct. Eng.*, 04017156.
Almeida, J. P., Tarquini, D., and Beyer, K. (2016). "Modelling approaches for inelastic behaviour of RC walls: Multi-level assessment and dependability of results." *Arch. Comput. Methods Eng.*, 23(1), 69–100.
Bimschas, M. (2010). "Displacement based seismic assessment of existing bridges in regions of moderate seismicity." Ph.D. thesis, ETH Zurich, Zürich, Switzerland.
Binici, B., and Mosalam, K. M. (2007). "Analysis of reinforced concrete columns retrofitted with fiber reinforced polymer lamina." *Compos. Part B Eng.*, 38(2), 265–276.
Biskinis, D., and Fardis, M. N. (2007). "Effect of lap splices on flexural resistance and cyclic deformation dapacity of RC members." *Beton- und Stahlbetonbau*, 102(S1), 51–59.
Biskinis, D., and Fardis, M. N. (2010a). "Deformations at flexural yielding of members with continuous or lap spliced bars." *Struct. Concr.*, 11(3), 127–138.
Biskinis, D., and Fardis, M. N. (2010b). "Flexure-controlled ultimate deformations of members with continuous or lap-spliced bars." *Struct. Concr.*, 11(2), 93–108.
Cairns, J. (1985). "Strength of compression splices: A reevaluation of test data." *ACI J.*, 82(4), 510–516.
Calabrese, A., Almeida, J. P., and Pinho, R. (2010). "Numerical issues in distributed inelasticity modeling of RC frame elements for seismic analysis." *J. Earthquake Eng.*, 14(S1), 38–68.
Canbay, E., and Frosch, R. J. (2005). "Bond strength of lap-spliced bars." *ACI Struct. J.*, 102(4), 605–614.
Chai, Y., Priestley, M., and Seible, F. (1991). "Seismic retrofit of circular bridge columns for enhanced flexural performance." *ACI Struct. J.*, 88(5), 572–584.
Cho, J., and Pincheira, J. A. (2006). "Inelastic analysis of reinforced concrete columns with short lap splices subjected to reversed cyclic loads." *ACI Struct. J.*, 103(2), 280–290.
Chowdhury, S. R., and Orakcal, K. (2012). "An analytical model for reinforced concrete columns with lap splices." *Eng. Struct.*, 43, 180–193.
Eligehausen, R., Popov, E. P., and Bertero, V. V. (1983). "Local bond stress-slip relationships of deformed bars under generalized excitations." *Rep. UCB/EERC-83/23*, Univ. of California, Berkeley, CA.
Elnady, E. M. M. (2008). "Seismic rehabilitation of RC structural walls." Ph.D. thesis, McMaster Univ., Hamilton, ON, Canada.
Esfahani, M. R., and Rangan, B. V. (1998). "Bond between normal strength and high-strength concrete (HSC) and reinforcing bars in splices in beams." *ACI Struct. J.*, 95(3), 272–280.
Esfahani, M. R., and Rangan, B. V. (2000). "Influence of transverse reinforcement on bond strength of tensile splices." *Cem. Concr. Compos.*, 22(3), 159–163.
fib (Federation Internationale du beton). (2012). "Model code 2010—Final draft, volume 1." *Technical Rep. FIB Bulletin 65*.
fib (Federation Internationale du beton). (2013). *Model code for concrete structures 2010*, Ernst and Sohn, Lausanne, Switzerland.
Gergely, P., and White, R. (1980). "Seismic design of lapped splices in reinforced concrete." *Proc., 7th World Conf. on Earthquake Engineering*, Vol. 4, Istanbul, Turkey, 281–288.
Girard, C., and Bastien, J. (2002). "Finite-element bond-slip model for concrete columns under cyclic loads." *J. Struct. Eng.*, 10.1061/(ASCE)0733-9445(2002)128:12(1502), 1502–1510.
Hannewald, P. (2013). "Seismic behavior of poorly detailed RC bridge piers." Ph.D. thesis, École Polytechnique Fédérale de Lausanne, Lausanne, Switzerland.
Hannewald, P., Bimschas, M., and Dazio, A. (2013). "Quasi-static cyclic tests on RC bridge piers with detailing deficiencies." *Institut fur Baustatik und Konstruktion, Bericht Nr. 352*, ETH Zurich, Zürich, Switzerland.
Harajli, M. H. (2009). "Bond stress-slip model for steel bars in unconfined or steel, FRC, or FRP confined concrete under cyclic loading." *J. Struct. Eng.*, 10.1061/(ASCE)0733-9445(2009)135:5(509), 509–518.
Harajli, M. H., Hamad, B. S., and Rteil, A. A. (2004). "Effect of confinement on bond strength between steel bars and concrete." *ACI Struct. J.*, 101(5), 595–603.
Harajli, M. H., and Mabsout, M. E. (2002). "Evaluation of bond strength of steel reinforcing bars in plain and fiber-reinforced concrete." *ACI Struct. J.*, 99(4), 509–517.
Hognestad, E., Hanson, N. W., and McHenry, D. (1955). "Concrete stress distribution in ultimate strength design." *ACI J. Proc.*, 52(12), 455–480.
Ichinose, T., Kanayama, Y., Inoue, Y., and Bolander, J. E. (2004). "Size effect on bond strength of deformed bars." *Constr. Build. Mater.*, 18(7), 549–558.
Kim, T.-H., Kim, B.-S., Chung, Y.-S., and Shin, H. M. (2006). "Seismic performance assessment of reinforced concrete bridge piers with lap splices." *Eng. Struct.*, 28(6), 935–945.
Kim, T.-H., Shin, H. M., Chung, Y.-S., and Hong, H.-K. (2009). "Seismic performance assessment of reinforced concrete bridge columns with lap splices using shaking table tests." *Mag. Concr. Res.*, 61(9), 705–719.
Kupfer, H., Hilsdorf, H. K., and Rusch, H. (1969). "Behavior of concrete under biaxial stresses." *ACI J.*, 66(8), 656–666.
Layssi, H., and Mitchell, D. (2012). "Experiments on seismic retrofit and repair of reinforced concrete shear walls." *Proc., 6th Int. Conf. on FRP Composites in Civil Engineering—CICE*, Rome, 1–8.
Lettow, S., and Eligehausen, R. (2006). "FIB task Group 4.5: Formulation of application rules for lap splices in the new model code." *Technical Presentation*, Univ. of California at Berkeley, Berkeley, CA.
Lowes, L. N., Lehman, D. E., Birely, A. C., Kuchma, D. A., Marley, K. P., and Hart, C. R. (2012). "Earthquake response of slender planar concrete walls with modern detailing." *Eng. Struct.*, 43, 31–47.
Lowes, L. N., Moehle, J. P., and Govindjee, S. (2004). "Concrete-steel bond model for use in finite element modeling of reinforced concrete structures." *ACI Struct. J.*, 101(4), 501–511.
Lukose, K., Gergely, P., and White, R. (1982). "Behavior of reinforced concrete lapped splices for inelastic cyclic loading." *ACI J. Proc.*, 79(5), 355–365.
Mander, J. B., Priestley, M. J. N., and Park, R. (1988). "Observed stress-strain behavior of confined concrete." *J. Struct. Eng.*, 10.1061/(ASCE)0733-9445(1988)114:8(1827), 1827–1849.
Melek, M., and Wallace, J. W. (2004). "Cyclic behavior of columns with short lap splices." *ACI Struct. J.*, 101(6), 802–811.
Ngo, D., and Scordelis, A. C. (1967). "Finite element analysis of reinforced concrete beams." *ACI J.*, 64(3), 152–163.
Nilson, A. H. (1972). "Internal measurements of bond slip." *ACI J.*, 69(7), 439–441.
Orangun, C. O., Jirsa, J. O., and Breen, J. E. (1977). "A reevaluation of test data on development length and splices." *ACI J.*, 74(3), 114–122.
Palermo, D., and Vecchio, F. J. (2003). "Compression field modeling of reinforced concrete subjected to reverse loading: Formulation." *ACI Struct. J.*, 100(5), 616–625.
Palermo, D., and Vecchio, F. J. (2004). "Compression field modeling of reinforced concrete subjected to reverse loading: Verification." *ACI Struct. J.*, 101(2), 155–164.
Palermo, D., and Vecchio, F. J. (2007). "Simulation of cyclically loaded concrete structures based on the finite-element method." *J. Struct. Eng.*, 10.1061/(ASCE)0733-9445(2007)133:5(728), 728–738.
Park, R., Priestley, M. J. N., and Gill, W. D. (1982). "Ductility of square-confined concrete columns." *J. Struct. Div.*, 108(4), 929–950.
Paulay, T. (1982). "Lapped splices in earthquake-resisting columns." *ACI J.*, 79(6), 458–469.
Paulay, T., and Priestley, M. J. N. (1992). *Seismic design of reinforced concrete and masonry buildings*, Wiley, New York.
Popovics, S. (1973). "A numerical approach to the complete stress-strain curve of concrete." *Cem. Concr. Res.*, 3(5), 583–599.
Priestley, M. J. N., Calvi, G. M., and Kowalsky, M. J. (2007). *Displacement-based seismic design of structures*, IUSS Press, Pavia, Italy.

Priestley, M. J. N., Seible, F., and Calvi, G. M. (1996). *Seismic design and retrofit of bridges*, Wiley, New York.
Pugh, J. S. (2012). "Numerical simulation of walls and seismic design recommendations for walled buildings." Ph.D. thesis, Univ. of Washington, Washington, DC.
Richart, F. E., Brandtzaeg, A., and Brown, R. L. (1928). *A study of the failure of concrete under combined compressive stresses*, Univ. of Illinois, Urbana, IL.
Sakurada, T., Morohashi, N., and Tanaka, R. (1993). "Effect of transverse reinforcement on bond splitting strength of lap splices." *Trans. Jpn. Concr. Inst.*, 15, 573–580.
Seckin, M. (1982). "Hysteretic behaviour of cast-in-place exterior beam column sub-assemblies." Ph.D. thesis, Dept. of Civil Engineering, Univ. of Toronto, Toronto.
Sozen, M., and Moehle, J. (1990). "Development and lap-splice lengths for deformed reinforcing bars in concrete." *Technical Rep. to Portland Cement Association*, Urbana, IL.
Sparling, B., and Rezansoff, T. (1986). "The effect of confinement on lap splices in reversed cyclic loading." *Can. J. Civil Eng.*, 13(6), 681–692.
Syntzirma, D. V., and Pantazopoulou, S. J. (2006). "Deformation capacity of RC members with brittle details under cyclic loads." *Concr. Int.*, 236, 1–22.
Talaat, M. M., and Mosalam, K. M. (2008). "Computational modeling of progressive collapse in reinforced concrete frame structures." *PEER Rep. 2007/10*, Pacific Earthquake Engineering Research Center, Berkeley, CA.
U.S. Federal Emergency Management Agency. (2000). "Prestandard and commentary for the seismic rehabilitation of buildings." *FEMA 356*, Washington, DC.
Valluvan, R., Kreger, M. E., and Jirsa, J. O. (1993). "Strengthening of column splices for seismic retrofit of nonductile reinforced concrete frames." *ACI Struct. J.*, 90(4), 432–440.
Vecchio, F. J. (1999). "Towards cyclic load modeling of reinforced concrete." *ACI Struct. J.*, 96(2), 193–202.
Vecchio, F. J., and Collins, M. P. (1986). "The modified compression-field theory for reinforced concrete elements subjected to shear." *ACI J.*, 83(2), 219–231.
VecTor2 [Computer software]. VecTor Analysis Group, Toronto.
Xiao, Y., and Ma, R. (1997). "Seismic retrofit of RC circular columns using prefabricated composite jacketing." *J. Struct. Eng.*, 10.1061/(ASCE)0733-9445(1997)123:10(1357), 1357–1364.
Zuo, J., and Darwin, D. (2000). "Splice strength of conventional and high relative rib area bars in normal and high-strength concrete." *ACI Struct. J.*, 97(4), 630–641.